Synthesis, Characterization and Bioactive Study of Borosilicate Sol-Gel Glass

Khairy M. Tohamy [1], Islam E. Soliman [1], Asem E. Motawea [2], Mohamed A. Aboelnasr [1*]

[1.] Biophysics Branch, Faculty of Science, Al-Azhar University, Nasr City 11884, Cairo, Egypt
[2.] Physics Department, Faculty of Science, Al-Azhar University, Nasr City 11884, Cairo, Egypt
*abomalk3939@gmail.com

Abstract: Silicon-boron based glass was prepared by sol gel method. This bioactive glass (70-x) SiO_2-$6P_2O_5$-$24CaO$ and (x) B_2O_3 in which SiO_2 substituted by B_2O_3 with variated values x = 0, 5, 10, 15, 20 and 25 wt %. The morphology of the 600 ^{0}C heat treated samples was characterized through SEM, EDX, XRD and FTIR. The bioactive glass have been analysed in vetro test. The results indicate that after 15 days of immersion, the microstructure of the sample with 15 wt% B_2O_3 is quite close to that of dry human trabecular bone.
[Tohamy KM, Soliman IE, Motawea AE, Aboelnasr MA. **Synthesis, Characterization and Bioactive Study of Borosilicate Sol-Gel Glass.** *Nat Sci* 2015;13(8):145-154]. (ISSN: 1545-0740). http://www.sciencepub.net/nature. 23

Keywords: sol-gel, borosilicate, bioactive glass, hydroxyapatite

1. Introduction

In the recent years bioactive glasses have attracted much interest as new materials used in numerous biomedical and research applications with high potential as scaffold materials. Silica- and phosphate-based glasses were found to be bioactive material [1–3] due to its ability to form bonelike apatite layer on its surface when interacting with host medium. The sol–gel route was introduced in early 1990s as an alternative synthesis method for this type of materials [1, 4-6]. It was shown that glasses obtained by sol–gel route are of higher homogeneity and purity, and can be prepared at lower temperature and with a better control of their structure and morphology than in the case of melt quenching method [4- 7].

The key to form a stable bond between the bone and a synthetic material is the precipitation of an apatite layer on the surface of the synthetic material which is responsible for its bioactivity [8, 9]. For tissue engineering applications it is necessary to increase the nucleation and growth of hydroxyapatite (HA) on the surface of the bio-glass in a precise reaction time in body environment, not to slow, because of the difficulty to match the rate of new tissue formation with the degradation rate of scaffolds, and however not too fast, because the weak HA-like layer product may result in an excessive decrease in the strength [10, 11].

For four decades, bioactive glasses in the system SiO_2–P_2O_5–CaO have been one of the most widely studied materials for biomedical applications [12–15]. It was also reported that the addition of the classical network former B_2O_3 to SiO_2–CaO–P_2O_5–Na_2O bioactive glass system generally leads to glass-ceramic materials that also present bioactivity [16]. One of the principal proposals in the development of glass-ceramics for biomedical applications is the possibility of improving the mechanical properties of their parent glasses. It was shown that the ratio between tetrahedral and trigonal boron species can influence the mechanical strength of a glass system owing to the fact that boron speciation plays a dominant role in controlling the fragility of the samples [17]. Boron can be considered as potential stimulating agent for bone tissue engineering. It was shown that boron affects the RNA synthesis in fibroblast cells.Moreover, dietary boron can stimulate bone formation [18, 19].

Therefore boron has been introduced to bioactive silicate glasses in an attempt to improve the bioactivity of the glasses and the structure of a material that may be suitable for biomedical applications [10,20-22]. Moreover, the B_2O_3-containing bioactive glasses have attracted the interest in the past years for potential biomedical applications in tissue engineering as scaffolds material, because of their lower chemical durability, faster and more completely conversion to hydroxyapatite when they are immersed in simulated body fluid [11,23,24].

The present study was focused on the sol–gel synthesis, structural characterization and in-vitro behavior of samples that follow the [(70-X) SiO_2-$6P_2O_5$-24CaO-(X) B_2O_3, X= 0, 5, 10, 15, 20 and 25%] composition.

2. Material and Methods

Tetraethyl orthosilicate (TEOS), calcium nitrate tetrahydrate $Ca(NO)_3·H_2O$, triethyl phosphate (TEP) ($\geq$ 98%) and boric acid (H_3BO_3) were purchased from (Fluka). Ammonia solution, 35%, and nitric acid, 65%, were purchased from Merck, USA. Both nitric acid and ammonia solutions were diluted to 2M using distilled water.

Table 1. Different additive of B_2O_3 on the: SiO_2-CaO-P_2O_5

Glass	Glass base (wt %)			Additives
	SiO_2	CaO	P_2O_5	B_2O_3
G_0	70	24	6	---
G_5	65	24	6	5
G_{10}	60	24	6	10
G_{15}	55	24	6	15
G_{20}	50	24	6	20
G_{25}	45	24	6	25

2.1. Synthesis of gel powder

Bioactive glass samples were synthesized through alkali-mediated sol–gel method after aging for four days from Preparation [25, 26]. B_2O_3 were added to the glass compositions at the expense of SiO_2. Table (1) lists the nominal compositions and codes of the prepared glasses. Initially, tetraethyl orthosilicate, distilled water, 2M nitric acid (as a hydrolysis catalyst), were successively mixed in ethanol and the mixture was allowed to react for 45 min under continuous magnetic stirring for the acid hydrolysis of TEOS. The molar ratio of water /TEOS was fixed at 1/12 and volume ratio of water/nitric acid was fixed at 1/6.

Then appropriate amounts of series of reagents were added in the following sequence: Ca $(NO)_3 \cdot 4H_2O$, (TEP), allowing 45 min for each reagent to react completely. In another small piker dissolve boric acid in distilled water, the molar ratio of water: H_3BO_3 was fixed at 15:1 at temperature 40 ^{0}C for 30 min [27] under continuous magnetic stirring for the acid hydrolysis of H_3BO_3. Then add this piker to the first piker.

After the final addition, mixing was continued for 60 min to complete hydrolysis. After all this steps aging all samples for four days. 2M ammonia solution (a gelation catalyst) was dropped into the mixture. The mixture was then agitated with glass rode (like as mechanical stirrer) to prevent the formation of a bulk gel. Finally, each prepared gel was dried at 120 ^{o}C for 2 days in a drying oven. According to the results of the thermal analysis of the dry gels, which showed that there was no further weight loss above 600 ^{o}C, the gels was stabilized by heat treatment, at a constant heating rate of 10 ^{o}C min^{-1} up to 600 ^{o}C.

2.2. Glass characterization

Differential scanning calorimetry (DSC) and thermal gravimetric analysis (TGA) were carried out using a computerized SETARAM labsys™ TG-DSC thermal analysis system range of 25–1000 ^{o}C with a heating rate of 10 ^{0}C/min, XRD patterns of the samples have been measured using [Axs D8 ADVANCE] with [Cuk$_\alpha$ =1.54056 A^o] radiation. The maximum current and voltage is 40 mA and 40 Kv. Fourier transform infrared (FTIR) spectroscopy measurements were recorded at room temperature in the range 400 – 4000 cm^{-1}, with Model 580, Perkin-Elmer. The surface of the glass samples were examined by scanning electron microscope (model XL30, Philips) attached with element analysis of X-Ray (EDX) unit, with accelerating voltage 30 KV, magnification up to 400,000 x and its resolution is (3.5 nm). SEM micrographs was obtained after coating the samples with Gold using Edwareds 5150 sputter coating (England).

2.3. *In vitro* measurements

In vitro bioactivity of the glasses was investigated by immersion in simulated body fluid (SBF) solution at 37 ^{0}C as proposed by Kokubo et al. [28.29], In vitro bioactivity of the glasses reflected in their capability for formation of hydroxyapatite layer onto their surface [26]. SBF contains the same concentrations of inorganic ions as human plasma. We carried out in vitro studies by soaking powder samples (0.4 g) in SBF solution (60 ml, pH=7.4). The sample-SBF mixtures were immediately sealed into sterilized containers, and were stored in an incubator at 37 ^{0}C for t = 15 days [30]. After soaking, the samples were filtered, washed by distilled water, and dried in air. The surface changes were then investigated through XRD, SEM, and FTIR measurements.

3. Results and Discussion
3.1. Crystallization behavior of glass powder
3.1.1. Thermal analysis

DSC trace is a plot of heat flow changes of the glass as a function of temperature and used to determine temperatures at which phase transitions occur. TGA trace is a plot of mass changes of the glass as a function of temperature used to determine weight loss from the samples. The changes induced in the samples by increasing the temperature up to 1000 ^{o}C were evidenced by thermal analysis. For the sample with x= 0 and 15 mol % B_2O_3 according to DSC curves (Fig. 1), an endothermic peak was first observed around 139 ^{0}C and 163 ^{0}C accompanied by weight loss (7.4 % and 10.12 %) for G $_0$ and G$_{15}$ respectively. This is assigned to the removal of adsorbed water [31, 32].

The DSC exothermic peaks at 294°C and 303°C, accompanied by weight loss (20.61% and 20.11) for G_0 and G_{15} respectively, observed in TG curves, are related to decomposition of organic residues, while the endothermic peak at 569°C and 493 °C accompanied by weight loss (21.10% and 17.83%) for G_0 and G_{15} respectively, on the T_G curve is related to removal of residual nitrate groups [31-34].

Then little weight loss took place up to 800 °C [22]. Similar DSC curves were obtained for all samples. According to these results the as prepared samples were heat treated at 600 °C. All the results presented further will refer to 600 °C heat treated samples.

Finally, there is an exothermic peak appeared on DSC curves for all samples which located at 934, 786, 734 and 715 °C, for samples G_0, G_5, G_{15} and G_{25}, respectively. This was due to transformation of the glass into glass-ceramic. This is can be explained as follows; when B_2O_3 is substituting SiO_2 it can act as the nucleating agents and decrease the barrier energy of crystallization. This then leads to relieve the rigidity of the glass structure and causes the disruption in the network structure by newly forming ionic bonds between B and oxygen (Si–O–B) in SiO_4 tetrahedrons in the glassy network. These ionic bonds are weaker than the bonds formed between the two silicon ions and oxygen (Si−O−Si) in the glassy network structure (silicate chain) and therefore, a reduction in T_c was observed. This reduction shift leads to phase transition temperatures to a lower value [20], as shown in Fig. (1).

A second interest comes because boron has the smallest mass compared to other network forming elements (e.g. Si and P). Also, this cause more pores in the glass structure [33]. This change undoubtedly corresponded to the change in the nature of bonding in the structural network. Meanwhile, with increasing B_2O_3 content, both T_g and the onset of crystallization peak T_c shifted toward lower temperatures. This clearly corresponds to the theory that the network addition is charge balanced resulting in polymerization of silicate network and also decrease of the T_g [23, 36] as seen in Fig. (1).

3.1.2. X-ray diffraction analysis

According to X-ray diffractograms presented in Fig. (2), the obtained samples exhibit a dominant vitreous structure. It was noted that the presence of diffraction peak for G_{0b}, G_{5b}, G_{10b}, G_{15b} samples, which can be assigned to amorphous calcium phosphate phase (ACPs) with chemical formula $Ca_4O (PO_4)_2$ which also appears at 2θ = 29.4°, 31.8° and 32.8°corresponding to the (1 3 2), (2 1 2) and (1 0 3) reflections. This peak positions of XRD patterns in four samples matched well with the standard pattern of card (JCPDF 251137) [37]. With further increasing X, (20, 30 mol% B_2O_3) the patterns show no crystalline phases[22] ACPs are the first solid phases, precipitated after a rapid mixing of aqueous solutions containing ions of Ca^{2+} and PO_4^{3-} [38].
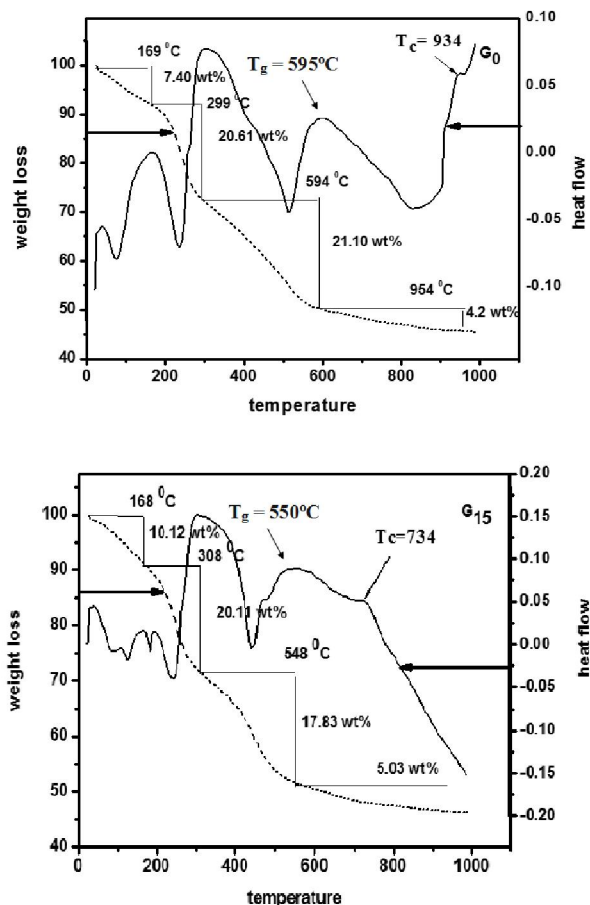

Figure 1. TGA and DSC curves of (a) G_0 and (b) G_{15} gel powder after at 120°C for 2 days

Figure (3) shows the XRD patterns for the samples after soaking in SBF for 15 days, there are four peaks at 2θ values of 22.8°, 25.76°, 31.8° and 32.96° develop after soaking in SBF for 15 days. These four peaks could be assigned to (1 1 1), (0 0 2), (2 1 1), (3 0 0) and indicating the formation of apatite layer on the surface of the gel glass according to the standard JCPDS file no. (82-1943), Wide diffraction peak at angles (2θ) ranging from 31.5° to 34° corresponds to the overlapping of (2 1 1), (1 1 2), (3 0 0) and (2 0 2) reflections of the well-crystallized HA [9, 10, 38]. The intensities of these reflection peaks of the HA phase increases with the enhancement of the accumulation of Ca^{2+} and PO_4^{3-} ions on the surface of the gel glass soaked in SBF [39].

There are also some low diffraction maxima at 2θ values 29.3°, 43.1°and 48.4°, that should be assigned to the reflections of (1 0 4), (2 0 2) and (1 1 6) of calcite according to the standard JCPDS card no (81-2027), These results indicate that calcite phase

formed during apatite layer growth, that may result from high release of calcium in ions the presence of hydrogen carbonate ions in SBF allowed the precipitation of calcite as described in the following the reaction:-

$$Ca^{2+} + 2HCO_3 \rightarrow CaCO_3 + CO_2 + H_2O$$

The calcite formation may be lowered by decreasing CaO concentration in the samples [41].

Based on XRD results (Fig. 2), the addition of B_2O_3 does not favors the crystalline calcium oxide phosphate phase formation in samples. Moreover, for x > 15 wt% B_2O_3 no sharp peaks were observed in the diffractograms. By analyzing the XRD patters obtained after t = 15 days of SBF immersion of samples one can observe that with increasing x, for t = 15 days, the intensity of the peaks characteristic for crystalline HA phase increases. For x = 15 mol% B_2O_3 the HA crystalline phase is more pronounced 15 days samples immersion in SBF. Moreover, the overall shape of the broad peak characteristic for the vitreous structure narrows in the samples immersed 15 days, probably due to a more pronounced tendency of local ordering than in the other investigated samples.
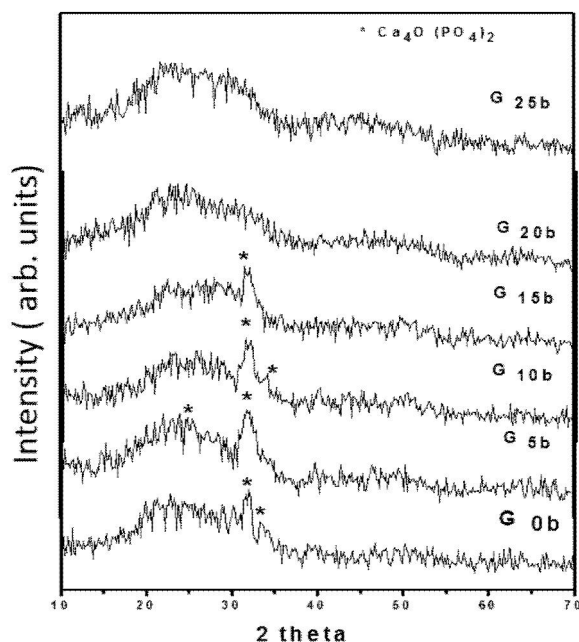

Figure 2. XRD patterns of sol-gel glass sample before soaking in SBF

Evaluation of apatite crystallinity by XRD

The crystallinity noted by X_C, corresponding to the fraction of crystalline apatite phase in the investigated volume of powder samples. The fraction

of crystalline phase (X_C %) in bio glass powders can be evaluated by the following equation [42, 43] :-

$$Xc = 1 - (V / I)$$

Where X_C is the crystallinity degree, I is the intensity of the main peak reflection and V is the intensity of the hollow between the main peak and the peak beside it.
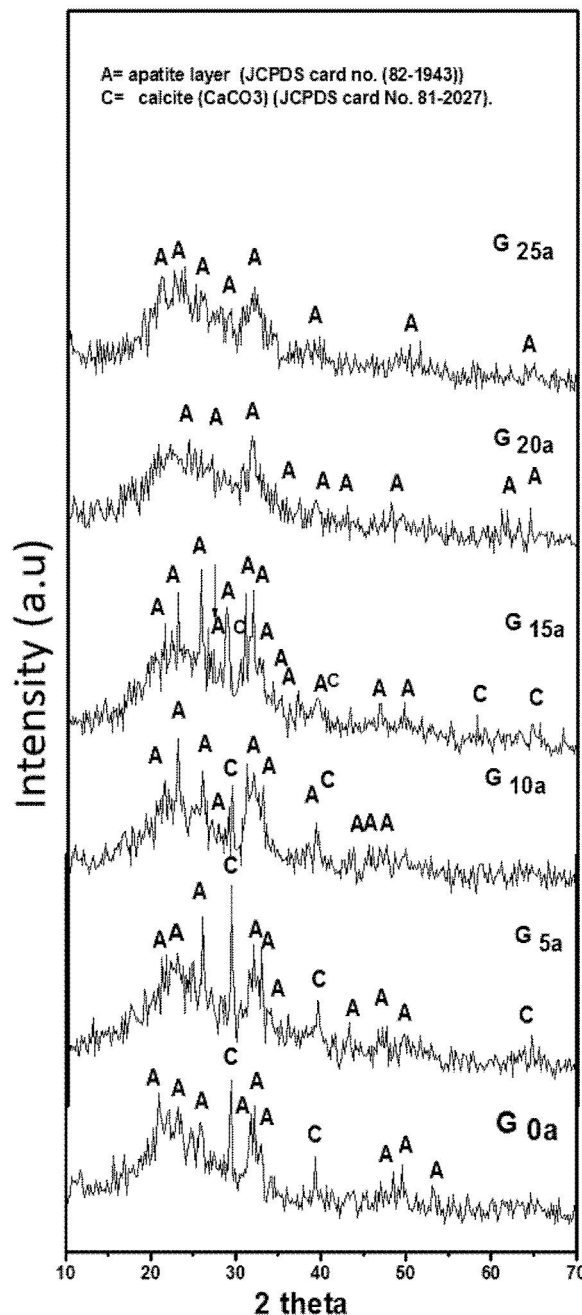

Figure 3. XRD patterns of gel glass after soaking in SBF

Figure (4) shows the dependence of X_c of the samples on B_2O_3 content. The sample G_{15a} exhibits higher X_c than the other samples with different additives of B_2O_3. The decrease of X_c for samples G_{20} and G_{25} may be attributed to the decrease of non-bridging oxygen as a result of increasing B-O as a unit of BO_4 (anomalous boron phenomenon) [44, 45].
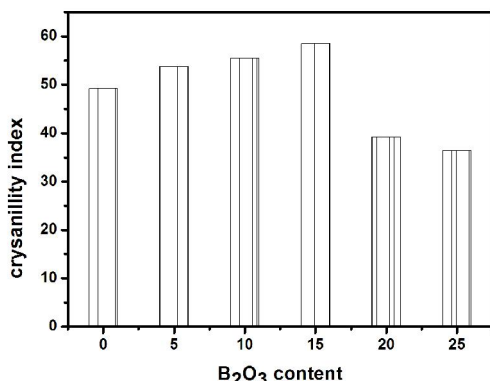

Figure 4. Crystallinity index (X_c XRD) of all glass samples against percentage of boron oxide, corresponds to the intensity of (2 1 1), (1 1 2) and (0 0 2).

3.1.3. FTIR analysis

FTIR absorption spectra of glass matrix (Fig. 5) show the two bands located at 459 and 676 cm^{-1} correspond to the vibrational mode of the bending of Si–O–Si and Si-O-B. The absorption band located at 805 cm^{-1} corresponds to Si–O symmetric stretch of bridging oxygen (BO) atoms between tetrahedrons. Absorption band at 955 cm^{-1} was observed, which can be attributed to Si-O$^-$ bond in (2NBO), where the band at ~1088 cm^{-1} has been assigned to asymmetric stretch vibrations of Si–O$^-$ bonds in (1NBO$_S$) tetrahedral units [25]. Beside the above mentioned bands, two bands located at 546 and 1034 cm^{-1} were observed and can be ascribed to P-O bending vibration of amorphous calcium phosphate (ACPs) and P-O stretching vibration, respectively. Band at 546 cm^{-1} that comes from the glass structure, evidenced also by the XRD measurements, ACPs are the first solid phases, precipitated after a rapid mixing of aqueous solutions containing ions of Ca^{2+} and PO_4^{3-} [36]. In addition, the band located at 1152cm^{-1} was assigned to P=O stretching vibration. The bands in the range ~ 1630–1650 cm^{-1} are due the deformation vibration of the H–O–H group.

The occurrence of these bands is confirmed by the presence of another broad band assigned to O–H stretching, located between ~ 3350 - 3600 cm^{-1}. The presence of these bands suggests that the diameter of the pores is higher than the atomic

interstices in a good agreement with the porous character of the sol–gel glasses [46].

The broad absorption band corresponding to the carbonate groups CO_3^{2-} was also detected at ~1300 - 1500 cm^{-1}. These CO_3^{2-} groups may be originated from CO_2 in air during the fabrication of sol-gel glass which is still remains after treatment at 600°C as small residual content.

Main changes imposed by increasing the addition of B_2O_3 in the studied samples are reflected in the FTIR spectra by the bands positioned at 465, 600, 690, 805, 940, 1081, 1195, and 1404 cm^{-1}, see Fig. (5). The band present at ~ 465 cm^{-1} was observed to be broadening by increasing B_2O_3 which can be due to the contribution from O–B–O bond-bending vibrations [27].
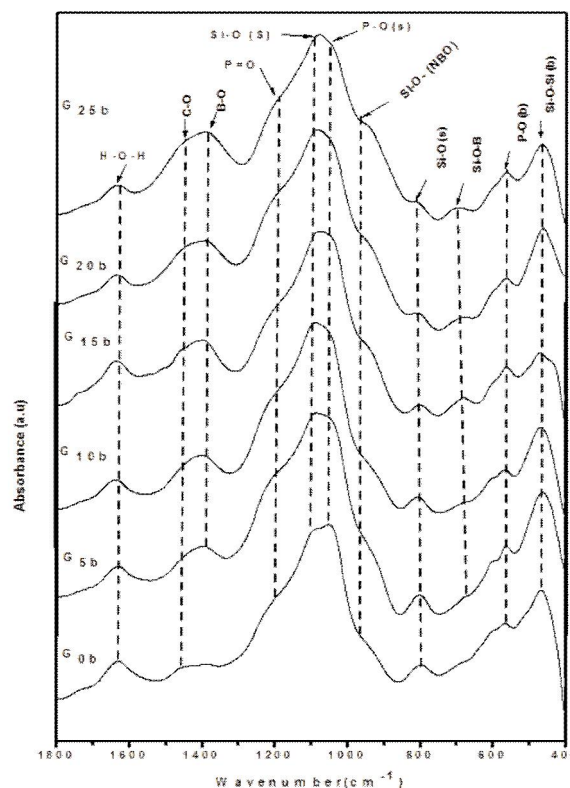

Figure (5). FTIR spectra of all synthesized sol-gel glasses with different amounts of B_2O_3 before soaking in SBF

The shoulder at 600 cm^{-1} presented in the reference sample G_{0b} represent P-O band in amorphous calcium phosphate phase gradually decrease with increase of B_2O_3. The addition of B_2O_3 to the SiO_2–P_2O_5–CaO system leads to decrease of this phase simultaneous and disappeared in two samples G_{20b}, G_{25b} with the rearrangement of silicon, phosphorous and boron atoms in the network [22, 27].

The band present at ~ 680 cm^{-1} increase with increasing B_2O_3 can be attributed to the formation of Si–O–B bonds [44] and may be due to B–O vibration in boroxyl ring [48].Also, the band present at ~800 can be attributed to Si–O [Bridging oxygen (BO)] decrease with increase B_2O_3 content. On the other hand, band located at 940 cm^{-1} which is assigned to Si–O[-] stretching in silicate tetrahedral units with three non-bridging oxygen (NBO) atoms and silanol group in **G_{0b}** sample. After addition of B_2O_3, this band appeared as clear shoulder due to linkages of stretching vibration B–O from BO_4 units with non-bridging oxygen (NBO) atoms and increases with increasing B_2O_3 contents from **G_{5b} to G_{25b}** samples [22, 28,49, 50].

The High frequency bands around 1430 cm^{-1} which increases with increasing of B_2O_3 from samples with containing CaO, these bands indicates the presence of NBOs which take the form as metaborate chains and rings, pyroborate and orthoborate groups [51]. The broad band located at 1640 cm^{-1} is assigned to the absorption band of molecular water.

The FTIR spectra recorded after 15 days of immersion in SBF show the positive role of boron oxide on the development of preferential crystalline HA phase supported by the following observations as shown in Fig. (6): (i) the double peak at 564 cm^{-1} and 603 cm^{-1} is present all over the compositional range [26] and (ii) two sharp peaks at 1070 cm^{-1} and 1090 cm^{-1} are present for samples with x = 20 and 25 wt % B_2O_3 as a contribution of HA phase and BO_4 units [12, 27, 33, 52].

The results obtained by FTIR after immersion in SBF revealed the positive role of boron ions on the bioactivity of the samples only for concentration lower than 20 wt % B_2O_3. Our data of FTIR suggest 15 wt % B_2O_3 as most favorable boron content added to $70SiO_2.6P_2O_5.24CaO$ composition that promotes HA phase development. [25],then more addition of boron content to system leading to inhibition of hydroxyapatite formation due to conversion of borons from 3- to 4- fold coordination, thus decrease of non-bridging oxygen's[35].

3.1.4. SEM Analysis

SEM coupled with Energy Dispersive X-ray (EDX) spectroscopy are also powerful techniques for visualizing (SEM) the new layer formed on the bioactive surface and to obtain information of the layer composition (EDX). Layer formed on a bioactive sol–gel glass and an ordered mesoporous material is schematically depicted.
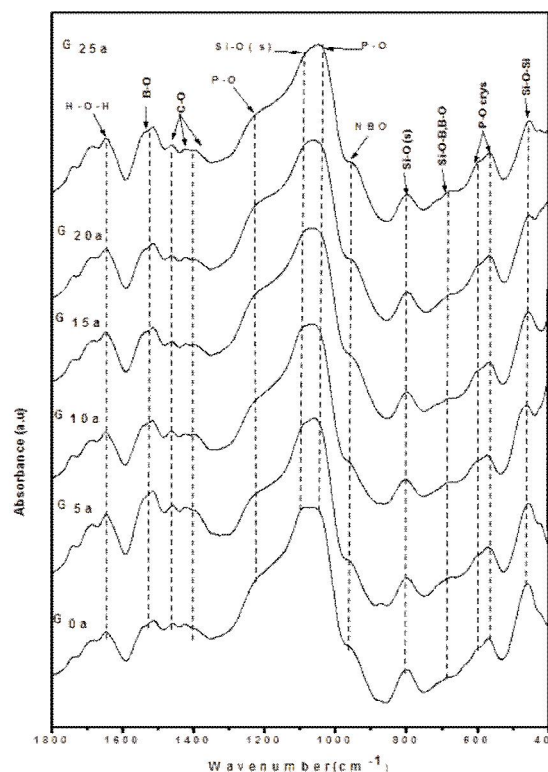

Figure 6. FTIR spectra of all synthesized sol-gel glasses with different amounts of B_2O_3 after soaking in SBF

The SEM image of the G_{15} (glass with 15% B_2O_3 before soaking) (Fig. (7)) is characterized by a nearly smooth surface formed on glass pellet. As seen in Fig. (7) there are one phase in sample before soaking in SBF, which can be assigned to calcium oxide phosphate Ca_4O $(PO_4)_2$ phase, evidenced also by the XRD measurements.

It is worth to note that after 15 days of immersion, the growth of white particles can be observed on its surface. So, glass surface becomes covered with a layer of spherical forms of apatite with dimensions of nearly 0.86-1.7 nm. An obvious difference in the surface morphology of all glass samples is observed after immersion in SBF, indicating the formation of apatite layer on the surface with different amounts. Also, the morphological structure of apatite-like layer varies with the boron oxide content of glasses.

A thick layer of apatite is noticed on the surface of G_{15} glass samples (Fig. 8), when compared to other glass samples, as data shown in Fig. (8). On surface of G_{0a}, G_{15a} and G_{25a}, crystalline aggregates are observed, but the size and density of the crystalline particles increase with addition of B_2O_3 up

to 15 % B_2O_3 content and diminishes with the enhancement of boron content.
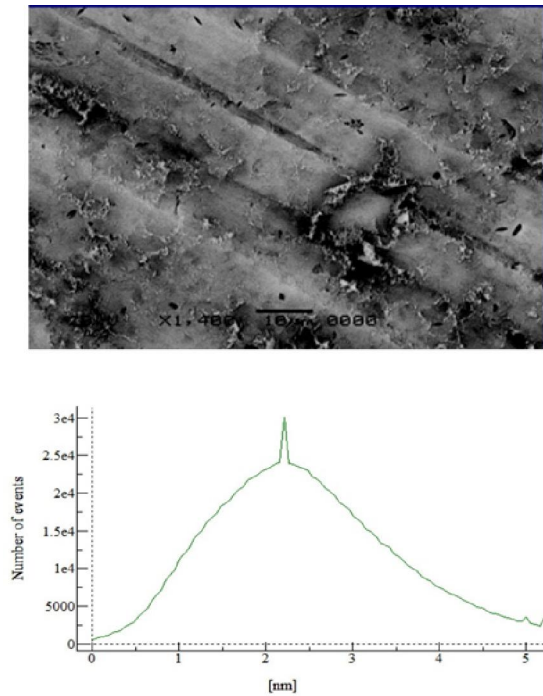

Figure 7. (Top) High magnification SEM image of bioactive glass sample G_{15b} before soaking in SBF showing the smooth sample surface. (Bottom) Roughness analysis on the SEM image indicating the formation of a single phase with a relatively narrow size distribution.
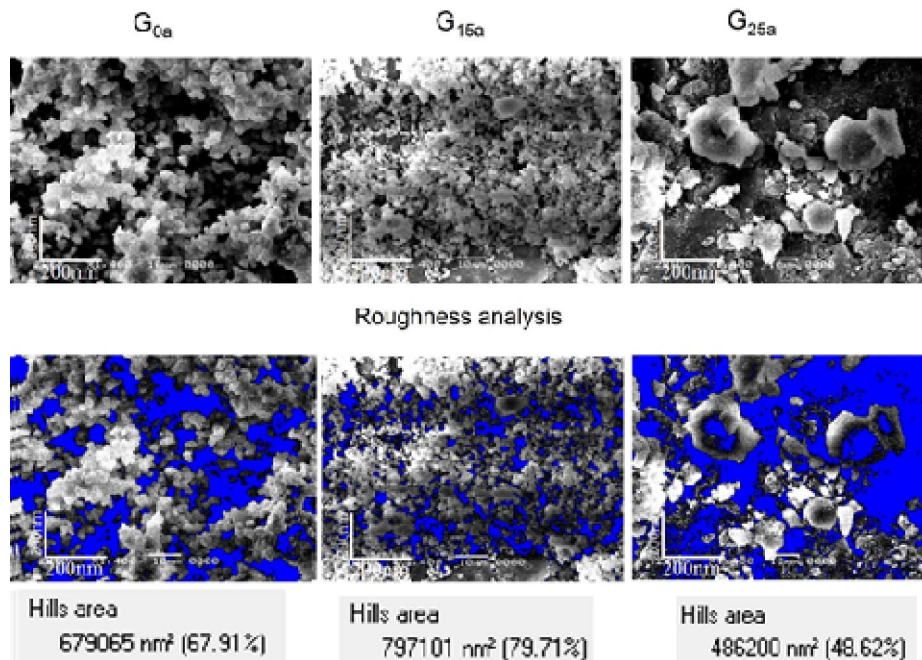

Figure 8. (Top) SEM images of the glass samples G_{0a}, G_{15a} and G_{25a}. (Bottom) The same SEM images after treatment with the flooding algorithm in SXWM software. The blue areas represent the free-apatite sample surface

Taking into account the shape of the structure newly appeared at the sample surface after immersion in SBF and the results of XRD, and FTIR analysis this can be taken as an additional evidence for the formation of an apatite type calcium phosphate layer.

In order to ensure that the observed particles on the sample surfaces are truly assigned to apatite layers, the EDX measurements have been conducted for all samples before and after the soaking in the SBF solution. The results of these measurements are displayed in Fig. (9), for G_{15} samples before and after soaking in SBF. Both spectra are characterized by a series of peaks characteristic for the elements Ca, O, Si, and P. A clear enhancement of the Ca and P peaks together with a reduction of the Si peak are observed after soaking in SBF for 15 days.
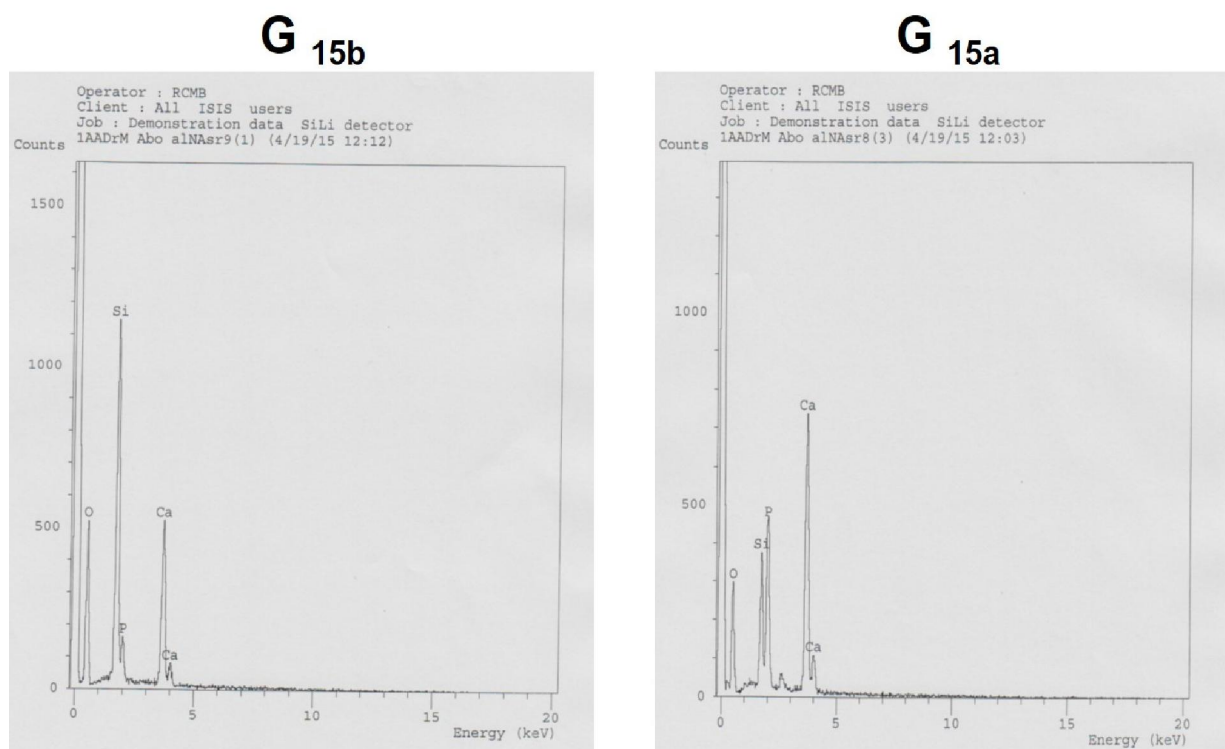

Figure 9. EDX spectra of G_{15b} and G_{15a} sample before and after soaking in SBF for 15 days, respectively. The Ca and P peaks are enhanced after soaking while the Si peak is reduced

4. Conclusion

B_2O_3 containing $70SiO_2-6P_2O_5-24CaO$ samples were synthesised using sol–gel method and a $600\ ^0C$ heat treatment of the obtained dried gels. Boron content strongly influences the local structure of samples and their bioactivity. With increasing B_2O_3Content up to 15 wt%B_2O_3 the glass-ceramic samples presents nanocrystallites assignable to CHA crystalline phases. A higher boron oxide content (X > 15 mol%) generates two important changes: (i) the structure passes from glass-ceramic to vitreous and (ii) the number of bridging oxygen units with less NBO atoms increases. The vitrification process inhibits the development of CHA and imposes the development of amorphous B-type CHA in sample with x= 25 wt% B_2O_3.

The results obtained after immersion in SBF revealed the positive role of boron ions on the bioactivity of the samples only for concentration lower than 20 mol% B_2O_3. Our data suggest 15 mol% B_2O_3 as most favorable boron content added to $70SiO_2.6P_2O_5.24CaO$ composition that promotes HA phase development. The sample with x = 15 wt% B_2O_3, after 5 days immersion in SBF has the highest porosity and the microstructure similar to that of dry human trabecular bone. Thus, in terms of our study, the B_2O_3 improves the bioactivity of a given composition as long as its amount is kept in the range of glass network modifier.

Corresponding Author:
Mohamed A. Aboelnasr
Biophysics Branch
Faculty of Science
Al-Azhar University, Nasr City 11884, Cairo, Egypt
E-mail: *abomalk3939@gmail.com

References

1. Hench, L.L., Bioceramics: from concept to clinic, J. Am. Ceram. Soc. 74(1991) 1487–1510.
2. Neo, M., Nakamura, T., Ohtsuki, C., Kokubo, T., Yamamuro, T.,"Apatite formation on three kinds of bioactive material at an early stage *in vivo*: A comparative study by transmission electron microscopy J.Biomed. Mater. Res. 27, (1993), 999-1006.
3. Knowles, J.C., "Phosphate based glasses for biomedical applications." J. Mater. Chem. 13, 2395 (2003).
4. Pereira, M.M., Hench, L.L., Mechanisms of hydroxyapatite formation on porous gel–silica substrates, J. Sol–Gel Sci. Technol. 7 (1996) 59–68.
5. Clupper D.C., Hench, L.L., Mecholsky, J.J, Strength and toughness of tape cast bioactive glass 45S5 following heat treatment, J. Eur. Ceram. Soc. 24 (2004) 2929–2934.
6. Li, R.,Clark, A.E.,Hench, L.L., An investigation of bioactive glass powders by sol–gel processing. J. Appl. Biomater. 2 (1991) 231–239.
7. Sepulveda, P., Jones, J.R., Hench, L.L., Characterisation of melt-derived 45S5 and sol–gel-derived 58S bioactive glasses, J. Biomed. Mater. Res. 58B (2001) 734–740.
8. Takadama, H., Kim, H.M., Kokubo, T., Nakamura T., X-ray photoelectron spectroscopy study on the process of apatite formation on a sodium silicate glass in simulated body fluid, J. Am. Ceram. Soc 85 (2002) 1933–1936.
9. Lopes, P.P., Leite Ferreira, B.J.M., Gomes, P.S., Correia, R.N, Fernandes, M. H., Fernandes, M.H.V., Silicate and borate glasses as composite fillers: a bioactivity and biocompatibility study, J. Mater. Sci: Mater. Med. 22 (2011) 1501–1510.
10. Deliormanli, A.M., In vitro assessment of degradation and bioactivity of robocast bioactive glass scaffolds in simulated body fluid, Ceram. Int. 38 (2012) 6435–6444.
11. Huang, W., Day, D.E., Kittiratanapiboon, K., Rahaman, M.N., Kinetics and mechanisms of the conversion of silicate (45S5), borate, and borosilicate glasses to hydroxyapatite in dilute phosphate solutions, J. Mater. Sci: Mater. Med. 17 (2006) 583–596.
12. Vallet-Regi, M., Ragel, C.V.,Salinas, A.J., Glasses with medical applications, Eur. J. Inorg. Chem. 6 (2003) 1029–1042.
13. Romian J., Padilla, S.,Vallet, M., Sol–gel glasses as precursors of bioactive glass ceramic, Chem. Mater. 15 (2003) 798–806.
14. Pereira, M.M., Clark, A.E., Hench, L.L., Calcium phosphate formation on sol–gel-derived bioactive glasses in vitro, J. Biomed. Mater. Res. 28 (1994) 693–698.
15. Sepulveda, P., Jones, J.R., Hench, L.L., In vitro dissolution of melt derived 45 S5 and sol–gel derived 58 S bioactive glasses, J. Biomed. Mater. Res. 61 (2002) 301–311.
16. Saranti, A., Koutselas, I, Karakassides, M.A., Bioactive glasses in the system $CaO–B_2O_3–P_2O_5$: preparation, structural study and in vitro evaluation, J. Non-Cryst. Solids 352 (2006) 390–398.
17. Zheng, Q., Potuzak, M., Mauro, J.C., Smedskjaer, M. M., Youngman, R.E.,Yue, Y., Composition-structure-property relationships in boroaluminosilicate glasses, J. Non-Cryst. Solids 358 (2012) 993–1002.
18. Nielsen FH. Is boron nutritionally relevant? Nutr Rev 2008;66(4):183.
19. Dzondo-Gadet M, Mayap-Nzietchueng R, Hess K, Nabet P, Belleville F,Dousset B. Action of boron at the molecular level. Biol Trace Elem Res 2002;85(1):23e33.
20. Fu, Q., Rahaman, M.N., Bal, B.S., Bonewald, L.F., Kuroki, K., Brown, R.F., Silicate, borosilicate, and borate bioactive glass scaffolds with control-lable degradation rate for bone tissue engineering applications. II. In vitro and in vivo biological evaluation, J. Biomed. Mater. Res. A 95(2010)172–179.
21. Fu, Q., Rahaman, M.N., Fu, H., Liu, X., Silicate, borosilicate, and borate bioactive glass scaffolds with controllable degradation rate for bone tissue engineering applications. I. Preparation and in vitro degradation, J. Biomed. Mater. Res. A 95 (2010) 164–171.
22. Yang, X., Zhang, L., Chen, X., Sun, X., Yang, G., Guo, X., Yang, H., Gao, C., Gou, Z., Incorporation of B_2O_3 in $CaO–SiO_2–P_2O_5$ bioactive glass system for improving strength of low-temperature co-fired porous glass ceramics, J. Non-Cryst. Solids 358 (2012) 1171–1179.
23. Day, D.E.,White, J., Brown R.F., McMenemin, K.D., Transformation of borate glasses into biologically useful materials, Glass Technol. 44(2003)75–81.
24. Yao, A., Wang, D.P., Huang, W., Rahaman, M.N., Day, D.E., In vitro bioactive characteristics of borate-based glasses with controllable degradation behavior, J. Am. Ceram. Soc. 90 (2007) 303–306.
25. El-Gohary M.I., Tohamy Kh. M. ,El-Okr M.M. ,Ali A. F., Soliman I. E.," Influence of composition on the in-vitro bioactivity of bioglass prepared by a quick alkali-mediated sol–gel method", Nature and Science 2013;11(3).
26. El-Kady, M. A., Ashraf, F. A., Rizk, R. A., Ahmed, M. M., "Synthesis, characterization and microbiological response of silver doped bioactive glass nanoparticles", Ceramics International, (2012) Vol. 38, pp. 177–188.
27. Lucacel Ciceo, R., Trandafir,D., Radu T., Ponta, O., Simon, V. " Synthesis, characterisation andin vitro evaluation of sol–gel derived $SiO_2–P_2O_5–CaO–B_2O_3$ bioactive system", Ceramics International, Vol. 40(2014), pp. 9517–9524.
28. Agathopoulos, S., Tulyaganov, D.U., Ventura, J.M.G., Kannan, S., Karakassides, M., Ferreira, J.M.F., Formation of hydroxyapatite onto glasses of the CaO–MgO–SiO2 system with B_2O_3,Na_2O, CaF_2 and P_2O_5additives, Biomaterials 27 (2006) 1832–1840.
29. Kokubo, T., Kushitani, H., Sakka S., Kitsugi T., Yamamuro T., Solutions able to reproduce in vivo

surface-structure changes in bioactive glass- ceramic A–W3, J. Biomed. Mater. Res. 24 (1990) 721–734.

30. Peitl, O., Dutra Zanotto, E., Hench, L.L., Highly bioactive P_2O_5–Na_2O–CaO–SiO_2 glass-ceramics, J. Non-Cryst. Solids 292 (2001) 115–126.

31. Trandafir, D.,Vasilescu, Simon M., S., Structural investigation of sol–gel derived SiO_2–GeO_2 noncrystalline and nanocomposite materials, J. Sol–gel Sci. Technol. 63 (2012) 425–434.

32. Carta, D., Knowles, J.C., Guerry, P., Smith, M.E., Newport, R.J., Sol–gel synthesis and structural characterisation of P_2O_5–B_2O_3–Na_2O glasses for biomedical applications, J. Mater. Chem. 19 (2009) 150–158.

33. Vulpoi, A., Baia, L., Simon, S., Simon, V., Silver effect on the structure of SiO_2–CaO–P_2O_5 ternary system, Mater. Sci. Eng. C 32 (2012) 178–183.

34. Laczka, M., Ciecinska, M., preparation, structure and properties of silicate-phosphate glasses obtained by means of Sol–gel method, J. Sol–gel Sci. Technol. 3 (1994) 219–227.

35. Abdelghany A.M.,ElBatal, H.A.,EzzElDin F.M.," Bone bonding ability behavior of some ternary borate glasses by immersion in sodium phosphate solution", Ceramics International 38 (2012) 1105–1113.

36. Srinivasan, S., Jayasree, R., Chennazhi, K.P., Nair, S.V., Jayakumar, R., Biocompatible alginate/nano bioactive glass ceramic composite scaffolds for periodontal tissue regeneration, Carbohydr. Polym. 87 (2012) 274–283.

37. Chen, C.C., Huang, T.H., Kao, C.T., Ding, S.J." Electrochemical study of the in vitro degradation of plasma-sprayed hydroxyapatite/bioactive glass composite coatings after heat treatment". Electrochimica Acta 50 (2004) 1023–1029.

38. Sergey V. Dorozhkin, " Amorphous calcium (ortho)phosphates" Acta Biomaterialia 6 (2010) 4457–4475.

39. Lee, DB, Song L., Kim,YJ. Effect of Ca and CaO on the high temperature oxidation of AZ91D Mg alloys, Mater. Trans. 49 (2008) 1084–1088.

40. Watts, S.J., Hill, R.G., O'Donnell, M.D., Law, R.V., J. Non-Cryst. Solids, (2010), Vol. 356, pp. 517-524.

41. Balamurugan, A., Balossier, G., Kannan, S., Michel J., Rebelo, A. H.S., Ferreira, Jose M.F., Acta Biomaterialia, (2007), Vol. 3, pp. 255-262.

42. Landi, E. and Tampieri, A., "Densification behavior and mechanism of synthetic hydroxyapatite", "Journal of European ceramic society", Vol.20, 2377-2387, (2000).

43. Pang, Y.X. and Bao, X., "Influence of temperature, ripening time and calcination on the morphology and crystallinity of hydroxyapatite nanoparticles", "Journal of the European Ceramic Society", Vol. 23, 1697–1704, (2003).

44. Wright, A.C., Feller, S.A., Hannon, A.C. (Eds.), Proc. 2nd Int. Conf. Borate Glasses, Crystal and Melts, Society of Glass Technology, Sheffield, UK, 1997.

45. Kamitsos, K.I., Infrared studies of borate glasses, Phys. Chem. Glasses 44 (2) (2003) 79–87.

46. Aguiar, H., Serra, J., Gonzãlez, P., Leȯòn, B., "Structural study of sol–gel silicate glasses by IR and Raman spectroscopies", J. Non-Cryst. Solids, Vol. 355(2009 pp. 475–480.

47. Xiu, T., Liu, Q., Wang, J., "Comparisons between surfactant-template mesoporous and conventional sol–gel-derived CaO–B_2O_3–SiO_2 glasses: Compositional, textural and in vitro bioactive properties, Journal of Solid State Chemistry", vol. 181(2008) pp. 863–870.

48. Muralidharan, P., Venkateswarlu, M., Satyanarayana, N., "Sol–gel synthesis, structural and ion transport studies of lithium borosilicate glasses", Solid State Ionics vol. 166(2004) pp. 27 – 38.

49. Boccaccini, A.R., Chen, Q., Lefebvre, L., Gremillard, L., Chevalier, J., (2007). "Sintering, crystallisation and biodegradation behaviour of Bioglass derived glass-ceramics", Faraday Discuss. Vol. 136 pp. 27–44.

50. Pryce, R.S., Hench, L.L., (2004). "Tailoring of bioactive glasses for the release of nitric oxide as an osteogenic stimulus", J. Mater. Chem., vol. 14 pp.2303-2310.

51. Manupriya, K.S., Thind, K., Singh, V., Kumar, G., Sharma D.P., Singh, et al., Compositional dependence of in-vitro bioactivity in sodium calcium borate glasses, J. Phys. Chem. Solids 70 (2009) 1137–11.

52. Melinte, G., Baia, L., Simon V., Simon, S., Hydrogen peroxide versuswater synthesis of bioglass-nanocrystalline hydroxyapatite composites,J. Mater. Sci. 46 (2011) 7393–7400.

8/23/2015